The Journal of Chemical Physics

Mid-IR spectroscopy of supercritical water: From dilute gas to dense fluid

Cite as: J. Chem. Phys. **150**, 054505 (2019); https://doi.org/10.1063/1.5079232
Submitted: 29 October 2018 . Accepted: 29 December 2018 . Published Online: 06 February 2019

Nicholas J. Hestand, Steven E. Strong, Liang Shi, and J. L. Skinner

AIP Publishing

The Journal of Chemical Physics ARTICLE scitation.org/journal/jcp

Mid-IR spectroscopy of supercritical water: From dilute gas to dense fluid

Cite as: J. Chem. Phys. 150, 054505 (2019); doi: 10.1063/1.5079232
Submitted: 29 October 2018 • Accepted: 29 December 2018 •
Published Online: 6 February 2019

Nicholas J. Hestand,[1,a] Steven E. Strong,[1,a] Liang Shi,[2] and J. L. Skinner[1,b]

AFFILIATIONS

[1] Institute for Molecular Engineering, University of Chicago, Chicago, Illinois 60637, USA
[2] School of Natural Sciences, University of California, Merced, California 95344, USA

[a] **Contributions**: N. J. Hestand and S. E. Strong contributed equally to this work.
[b] **Electronic mail:** jlskinner@uchicago.edu

ABSTRACT

Mixed quantum-classical methods are commonly used to calculate infrared spectra for condensed-phase systems. These methods have been applied to study water in a range of conditions from liquid to solid to supercooled. Here, we show that these methods also predict infrared line shapes in excellent agreement with experiments in supercritical water. Specifically, we study the OD stretching mode of dilute HOD in H_2O. We find no qualitative change in the spectrum upon passing through the near-critical region (Widom line) or the hydrogen-bond percolation line. At very low densities, the spectrum does change qualitatively, becoming rovibrational in character. We describe this rovibrational spectrum from the perspective of classical mechanics and provide a classical interpretation of the rovibrational line shape for both HOD and H_2O. This treatment is perhaps more accessible than the conventional quantum-mechanical treatment.

I. INTRODUCTION

The infrared (IR) spectrum of water provides a useful experimental probe of structure and hydrogen bonding in the fluid.[1] The IR spectrum of neat H_2O is complicated by coupling between OH chromophores, so one often measures the IR spectrum of the OD stretch of dilute HOD in H_2O instead.[1] The OD stretch is redshifted by about 1000 cm^{-1} from the OH stretch, decoupling it and simplifying the interpretation of the spectrum. However, the spectrum is still broad and difficult to interpret without the help of theoretical calculations. Because water's OD stretch vibration is at high frequency ($\sim$2600 $cm^{-1} \gg k_BT \sim 200$ cm^{-1}), a quantum-mechanical treatment is appropriate, but full-fledged electronic-structure based calculations are difficult and time consuming.[2–5] A common compromise is to use a mixed quantum-classical technique in which the low-frequency modes like translations and rotations/librations are treated classically using molecular dynamics (MD) simulations, while high-frequency modes are treated quantum mechanically within the framework of a vibrational exciton model.[6–15] This technique has been extensively used to compute theoretical spectra for liquid water,[7,8,10,11,15–18] and the same methods have been shown to be valid for various polymorphs of solid water,[6,19–23] as well as supercooled water.[24] Here, we show that this mixed quantum-classical method also extends to the supercritical region of water's phase diagram and performs well over a wide range of densities.

Supercritical fluids have many applications as industrial solvents, largely due to their tunable density.[25–27] Supercritical water, in particular, can, among other things, be used as an environmentally friendly solvent for hazardous waste cleanup.[28] However, the same properties that make supercritical water a useful solvent also make experiments difficult. Aside from the high pressures and temperatures required, supercritical water is a powerful oxidizer and corrodes many common components of experimental apparatus.[29–35] This difficulty makes theoretical predictions even more essential to understanding the properties of supercritical water.

As one tunes the density of supercritical water, one expects the IR spectrum to change qualitatively. At high

densities, hydrogen bonding weakens covalent OD bonds, leading to redshifted vibrational frequencies.[36–39] As the density decreases and hydrogen bonds weaken and break, the spectrum should blueshift. While the density is continuously tunable in supercritical fluids, there are features in the supercritical phase diagram, like the Widom and percolation lines, where one might expect the IR spectrum of water to change qualitatively.

The "Widom line" is an extension of the liquid-vapor coexistence line into the supercritical region.[40,41] It has been used extensively in the context of supercooled water as evidence of a nearby critical point,[24,41–43] and in the context of supercritical water as a dividing line between "gas-like" and "liquid-like" regions of the phase diagram.[44–47] As a sharp dividing line between gas-like and liquid-like "states," however, the concept of the Widom line is problematic because its location depends on the path taken through the phase diagram.[48,49] Moreover, some transitions that one would associate with a liquid-like to gas-like transition, like the breakdown of the hydrogen bonding network in water, do not occur at the Widom line.[50] Therefore, while the Widom line may be useful as evidence for a critical point, it would be beneficial to have a different construct that more accurately reflects the continuous nature of the liquid-like to gas-like transition. Here, we use the term "near-critical region," which is ambiguously defined by the region where the thermodynamic susceptibilities are large. This is similar in spirit to the "Widom delta,"[47,51] except that the near-critical region is intentionally ambiguous to more accurately describe the nature of the "transition" between two ambiguously defined states. While the term "near-critical region" is largely interchangeable with "Widom line" or "Widom delta," we feel that it better reflects the continuous and ambiguous nature of the transition.

In many simple molecular fluids like N_2 and O_2, the IR line shape broadens near the critical point.[52–54] This phenomenon, known as critical line broadening, occurs for systems in the motionally narrowed limit, where the line width depends on the relaxation time of the frequency-frequency correlation function.[55] In this limit, the line width depends on the dynamics of the system, which slow down near the critical point, resulting in a broader line shape. This has been well characterized through a mode-coupling theory for the frequency-frequency correlation function.[52,54] The IR line shape of water, on the other hand, is not in the motionally narrowed limit, but is inhomogeneously broadened, so that the line width depends only on the static frequency distribution. In this case, dynamics do not affect the line width,[55] so we do not expect to see critical line broadening. The IR line shape could, however, change qualitatively near the critical point for other reasons. For example, the IR line shape is sensitive to the hydrogen-bonding environment, which may change dramatically near the critical point, where the fluid changes most rapidly from liquid-like to gas-like. Likewise, one might expect the line shape to change upon crossing the percolation line, which describes the breakdown of the hydrogen-bonding network in the supercritical region.[50] There, the qualitative change in character of the hydrogen-bonding network might translate to a qualitative change in the IR line shape.

Here, we focus on the IR experiments of Franck and Roth, which probe the OD stretch of dilute HOD in H_2O.[29] They measured IR line shapes over a wide range of densities at 673 K, about 4% above the critical temperature. Interestingly, the spectrum changes very little as the density goes from 0.1 to 0.9 g/mL, displaying only a weak redshift of about 50 cm^{-1}. This is surprising, not only because they see no signatures of the critical point or percolation line but also because the redshift is relatively small. One at least expects a more substantial redshift at higher densities where hydrogen bonding is more prevalent. Our theoretical results are in good agreement with the experiment (Sec. III A), and we provide a microscopic understanding of the minimal density dependence (Sec. III B).

The IR line shape does, however, change qualitatively at very low densities (~0.05 g/mL), where it takes the characteristic rovibrational structure of the isolated HOD molecule.[29] Yoshida *et al.* captured this line shape well using a fully classical model.[56,57] The mixed quantum-classical method we use here also reproduces the low density spectrum well and extends to the high density regime without reparameterization. Yoshida *et al.* demonstrated that the features in the low density rovibrational spectrum are due to classical rotations, but the details remain unclear.[56,57] In neat H_2O, for example, there are two vibrational modes, the symmetric and antisymmetric stretches, but only the Q branch for the antisymmetric stretch is observed experimentally.[58] This can be understood in terms of quantum mechanical selection rules,[59,60] but these do not apply in our mixed quantum-classical model or the fully classical model.[56,57] Yoshida *et al.* suggest that the Q branch for the symmetric stretch is obscured by the P branch. Here, we show that the Q branch for the symmetric stretch is actually classically forbidden, due to an interesting application of the "tennis-racket theorem" of classical mechanics (Sec. III C).

II. METHODS

A. Simulation details

We perform classical molecular dynamics simulations with the TIP4P/2005 rigid water model.[61] We use the TIP4P/2005 model because its critical temperature and density (640 K and 0.310 g/mL) are quite close to the experimental numbers for water (647 K and 0.322 g/mL).[62,63] Intermolecular geometries are constrained with the SETTLE algorithm.[64] The dynamics are integrated using the leap-frog algorithm[65] with a 1 fs time step and a Nosé-Hoover thermostat with a 0.1 ps damping time.[66,67] We use periodic boundary conditions with the particle-mesh Ewald method for long range electrostatic interactions.[68] The simulations are performed with the GROMACS package.[69]

We simulate 500 water molecules at 673 K (400 °C) and at densities ranging from 1.5×10^{-3} g/mL to 1 g/mL. We study these conditions to allow comparisons with experiments at the same conditions.[29] We also perform simulations with 4000

water molecules to verify that the IR line shape is independent of the system size (data not shown), even near the critical point where correlations become long ranged. The simulations include 50 ps of equilibration time followed by 400 ps of data collection. At the lowest density (1.5×10^{-3} g/mL), we only simulate 100 water molecules because the simulation box is very large, making the particle-mesh Ewald calculation computationally expensive.

At low densities, the rarity of collisions raises potential issues in the MD simulation. Collisions allow equilibration through the redistribution of energy, so at low densities, equilibration is slow. We run longer simulations to test that our simulations are fully equilibrated. Further, MD thermostats do not generate exact Newtonian dynamics.[66,70] In dense liquids, where the dynamics are overdamped, the thermostatted dynamics are largely indistinguishable from Newtonian dynamics. At very low densities, where the molecules are mostly isolated, this may no longer be the case. We perform simulations at constant energy (NVE) to test that the thermostat does not affect the results.

We also perform simulations of explicit HOD molecules using in-house modifications to the LAMMPS software package,[71] which are available upon request. These simulations are largely identical in detail to the GROMACS simulations.

B. Spectroscopic calculations

We compute the IR line shape $\mathcal{I}(\omega)$ of the OD stretch of dilute HOD in H_2O using the mixed quantum-classical methods described in Refs. 12–15. In this approach, the line shape is given by the Fourier transform of the dipole correlation function $\phi(t)$ of the system, broadened by the average lifetime of a vibrational excitation T_1. We compute $\phi(t)$ according to Ref. 12, using the TIP4P spectroscopic maps[72] adapted for the TIP4P/2005 model.[24] Following others,[12] we assume an average vibrational lifetime of T_1 = 1.45 ps for the OD stretch, as determined from experiment.[73] We simulate neat liquid H_2O and average the spectrum over all OH chromophores, treating each as an implicit OD chromophore separately. This approach has been successfully used to model the spectroscopy of dilute HOD in H_2O at ambient conditions because the vibrational properties of the solute depend mostly on the dynamics of the solvent.[12,74–76] For all spectra presented here, we calculate the correlation function $\phi(t)$ for 20 ps with a time step of 10 fs and average over 760 choices of $t = 0$.

In Sec. III C, we also compute the IR spectrum of neat H_2O. There, we compute $\phi(t)$ according to Ref. 13 and use T_1 = 0.26 ps for the OH stretch.[77]

III. RESULTS AND DISCUSSION

A. The OD stretch in supercritical water

Franck and Roth measured experimental spectra of dilute HOD in H_2O at 673 K over a range of densities in the supercritical region of the phase diagram.[29] We compute spectra at the same conditions using the mixed quantum-classical method described in Sec. II B. A similar system was studied by Yoshida *et al.* using a purely classical method.[56,57] This method performs well at low densities. Because our method uses spectroscopic maps parameterized from electronic structure calculations, however, we are able to reproduce the experiment[29] over a wide range of densities (Fig. 1), even though the maps were parameterized for liquid water at ambient conditions.[72]

While the overall agreement with the experiment is very good, there are some disagreements at low density (0.1 g/mL). There, the theoretical result overestimates the spectral intensity at higher frequencies (Fig. 1). This is due to some combination of a failure of the spectroscopic map and a failure of the water model. Because the map was parametrized for liquid water, it does not quantitatively reproduce the properties of gas-phase water. The map predicts that the OD stretch of a gas-phase molecule is at 2767 cm^{-1},[72] while the experimental value is 40 cm^{-1} lower at 2727 cm^{-1}.[78] This bias to higher frequencies may be partly responsible for the high frequency tail seen at lower densities where there are more molecules in a gas-like environment. The high-frequency tail may also be due to a failure of the TIP4P/2005 water model, which is "a general purpose model for the condensed phases of water,"[61] and was not parametrized to reproduce gas-phase properties of water. If, for example, the TIP4P/2005 water model underestimates the amount of hydrogen bonding in low-density supercritical water, then the theoretical spectrum would

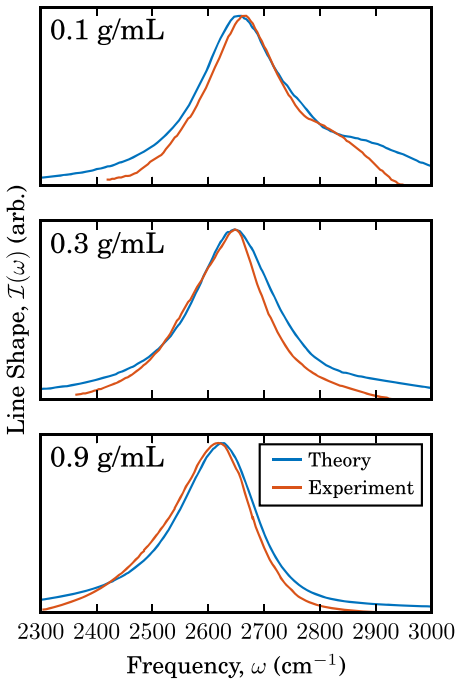

FIG. 1. The IR spectra of the OD stretch of dilute HOD in H_2O at 673 K and various densities. The theoretical spectra (blue) approximate the experimental[29] ones (orange) quite well. The theoretical spectra are normalized to have the same peak height as the experimental spectra.

overestimate the spectral intensity at higher frequencies, as we observe.

Overall, the spectral line shapes appear very similar to those observed in water at ambient conditions.[74–76,79] At high densities, the peaks are broad and featureless, reflecting the heterogeneous environment experienced by OD chromophores. As the density decreases, this inhomogeneous broadening is gradually replaced by a different type of inhomogeneous broadening, where the distribution in frequencies stems from a distribution in rotational energy (Sec. III B). At lower densities, where collisions are infrequent on the time scale of a vibrational lifetime (T_1 = 1.45 ps), rotational transitions can occur simultaneously with vibrational excitations, broadening the vibrational peaks. At higher densities, collisions are frequent and rotational energy is constantly scrambled between states, so this broadening mechanism is not important. The high-frequency shoulder at 0.1 g/mL (Fig. 1) originates from this rotational broadening and is attributed to the high-frequency R branch of the rovibrational spectrum of gas-like molecules.

At even lower densities (1.65×10^{-2} g/mL), the full rovibrational spectrum emerges (Fig. 2). The single broad peak seen at higher densities is replaced by two broad peaks surrounding a sharp central peak (Fig. 2). This rovibrational structure is well understood and arises due to transitions between quantized rotational levels that occur coincident with vibrational excitation.[60] For an asymmetric rigid rotor like HOD, quantum selection rules dictate that changes in the rotational quantum number J are restricted to $\Delta J = -1, 0, +1$, resulting in the three peaks shown in Fig. 2. In order of increasing frequency, these peaks are referred to as the P, Q, and R branches.[60] The experimental spectrum in Fig. 2 partially resolves the fine structure of these peaks, but the mixed quantum-classical method used here does not because rotational states are not quantized. The fact that this method can capture the rovibrational line shape at all may surprise the reader and will be discussed in considerable detail in Sec. III C.

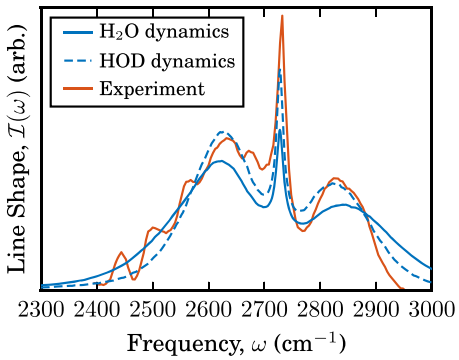

FIG. 2. The experimental IR spectrum[29] (orange) of the OD stretch of dilute HOD in H_2O at 673 K and 1.65×10^{-2} g/mL, compared to theoretical spectra (blue) at the same conditions. When the spectrum is computed with explicit HOD molecules (dashed blue), the agreement is significantly better than when computed with implicit HOD molecules (solid blue). The theoretical spectra are shifted by 40 cm^{-1} to account for the failures of the spectroscopic map at low densities and normalized by the area under the curve (see text). Even though the theoretical spectrum (blue) treats rotations classically, it still captures the rovibrational structure of the spectrum.

Apart from the fine structure, we find good agreement between the experimental spectrum and the theoretical prediction (Fig. 2). At this low density, there are several important factors that must be taken into account. First, as discussed in Sec. II B, it is common practice to simulate neat H_2O instead of explicitly simulating dilute HOD in H_2O.[12,16,74–76] We find this approach to be valid for supercritical water as well at the higher densities shown in Fig. 1 (data not shown). In very dilute systems (Fig. 2), however, the difference in the moments of inertia of H_2O and HOD has a significant effect on the free rotational dynamics of the molecule.[57] By computing the theoretical spectrum from an MD simulation of explicit HOD molecules, we find much better agreement with the experiment (Fig. 2). In doing so, we approximate the true dynamics of dilute HOD in H_2O with those of neat HOD, but at these low densities, the effect of the "solvent" should be minimal. Further, the computational cost of simulating true dilute HOD in H_2O is prohibitive. Second, the spectra in Fig. 1 are normalized by their peak height to enable comparisons with the experiment. In Fig. 2, however, there are three different peaks, and it is unclear which one should be normalized to the experiment. Instead, we normalize the spectra by the area under the curve. Finally, since the maps are not parametrized for these gas-phase environments, there is a systematic shift in the frequency which corresponds to the 40 cm^{-1} difference between the experimental gas-phase OD frequency (2727 cm^{-1}) and the gas-phase frequency of the spectroscopic map (2767 cm^{-1}). In Fig. 2, we subtract this 40 cm^{-1} shift from the theoretical spectra.

B. Density dependence of the IR spectrum

Besides small disagreements in the tails of the line shape, the theoretical spectra match the experiment remarkably well over a wide range of densities (Figs. 1 and 2). As a function of density, the most noticeable change in the spectrum is the development of the rovibrational line shape (Fig. 2). Figure 3(a) overlays the theoretical spectra as a function of density and reveals two other important changes: the intensity increases dramatically with increasing density, and the spectra redshift. The increasing intensity is a non-Condon effect, where the transition dipole moment depends on the molecular environment: water molecules in the condensed phase are "brighter" than those in the gas phase.[80,81] The redshift is caused by the increasing hydrogen bonding at higher densities, which weakens the OD bonds and lowers their characteristic frequencies.[36–39]

We quantify the redshift using the peak position, which is the frequency of maximum intensity [Fig. 3(b)]. The peak position we observe follows the same trend as the experiment and is semi-quantitative except at low density where the 40 cm^{-1} shift in the spectroscopic map becomes important, as discussed above. In Fig. 3, this shift is not removed.

Surprisingly, the peak position only redshifts by about 50 cm^{-1} from 0.1 to 0.9 g/mL. This contradicts both of the

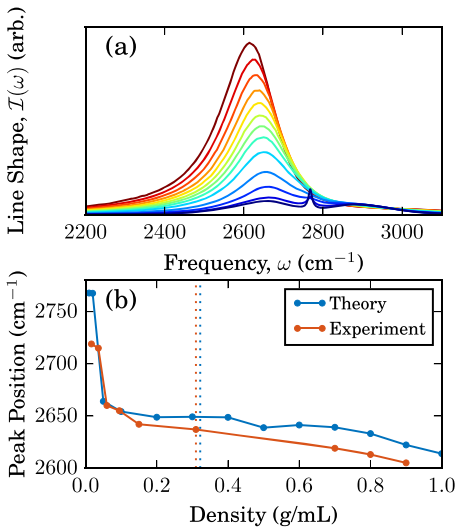

FIG. 3. (a) The theoretical IR spectra of the OD stretch of dilute HOD in H_2O at 673 K redshifts as a function of density, from low density (blue, 0.01 g/mL) to high density (red, 1.0 g/mL). The spectra are at the same densities as the points in panel (b). (b) The peak position, or frequency of maximum intensity, as a function of water density. Neither the experimental[29] (orange) nor the theoretical result (blue) show any change in behavior upon crossing the critical density (dotted lines).

expectations discussed in Sec. I: (1) that the spectra might change near the critical point or percolation transition and (2) that the spectrum should redshift more dramatically. Indeed, the total experimental redshift is more than 100 cm^{-1} over the full range of densities studied.[29] Barring any dramatic changes near the critical point or percolation line, one expects the peak position to redshift smoothly over this range, as hydrogen bonding increases.[36–39,50,82,83] Instead, the peak position jumps abruptly at low density (~0.05 g/mL) and redshifts only weakly at higher densities [Fig. 3(b)]. One may be tempted to attribute the jump in peak position at 0.05 g/mL to the near-critical region or percolation line, but these are both at significantly higher densities.[70] Since these simulations and experiments are at constant temperature, the near-critical region roughly follows the constant temperature Widom line.

The jump in the peak position is instead related to the emergence of the rovibrational line shape at low densities (<0.05 g/mL). By coincidence, the low-frequency P branch of the rovibrational spectrum is at roughly the same frequency as the inhomogeneously broadened peak at higher densities. As a result, at intermediate densities, the peak position is a weak function of the density because the rotational P branch transitions smoothly into the high-density inhomogeneously broadened peak. The jump in peak position seen in Fig. 3(b) is not due to a sharp transition between these two regimes, but simply caused by the central Q branch overtaking the P branch, shifting the peak position discontinuously.

Neither our IR nor the unpolarized Raman spectra (data not shown)[84] change qualitatively upon crossing through the near-critical region. This disagrees with some experimental results,[85–87] possibly due to the difficulty of performing experiments on supercritical water, especially near the critical point. We also find no evidence of crossing the percolation line. The breakdown of the hydrogen-bonding network that occurs upon crossing the percolation line is a collective phenomenon, while the effect of hydrogen bonding on the stretching frequency is much more local. While hydrogen bonding is cooperative,[88] the effect largely cancels out[89] except in exotic structures like hydrogen-bonded chains.[90,91] There is evidence that these structures are not important in supercritical water, even in the near-critical region where the density is low and fluctuations dominate.[50] As a result, the stretching of an OD chromophore is largely unaffected by any large-scale collective changes in the fluid or hydrogen-bonding network as one crosses through the near-critical region or the percolation line. Rather, the spectrum changes smoothly upon passing by these features of the phase diagram.

This may seem to contradict evidence from simulations that the IR spectrum changes qualitatively near the postulated liquid-liquid critical point in supercooled water.[24] There, the IR intensity varies sharply upon crossing the Widom line at constant pressure. Further from the critical point, however, where the theoretical spectra are in good agreement with experimental measurements,[92–94] the variation is much less dramatic. Here, we are studying supercritical water at temperatures only 33 K (1.05T_c) from the critical point, close enough that the thermal susceptibilities have pronounced maxima along isobars.[50,95,96] So, any effect in the IR spectrum should be obvious, but there are no qualitative changes in Fig. 3(b). To verify this, we also perform simulations closer to the critical point, at 1.01T_c, and find results that are qualitatively identical to those shown in Fig. 3(b).

The discrepancy with observations in supercooled water stems from the following difference. Experiments and simulations in supercooled water are done as a function of temperature, while those in supercritical water are done as a function of density. As one tunes the temperature near a critical point, the density changes abruptly, and the IR spectrum changes with it.[24] If the density is tuned, on the other hand, there is no abrupt change in density because it is the control parameter, so there is likewise no abrupt change in the IR spectrum. Here, we choose to study the system as a function of density because this is how the experiments are done.[29]

C. A classical perspective on the rovibrational spectrum

One important feature of the experiment that is missing in the theoretical spectrum is the rotational fine structure. The experimental spectrum in Fig. 2 shows some rotational fine structure in the P-branch ($\Delta J = -1$), and others have been able to better resolve the structure.[58,78] The quantum-mechanical origin of this rovibrational line shape has been understood for almost a century,[59,60,97] but it may surprise the reader that the mixed quantum-classical spectrum still captures the overall spectral envelope (Fig. 2).

The shape cannot come from transitions between quantized rotational states because rotational states are not quantized in our model. Instead, the P and R branches arise from the *classical* rotations of the water molecules. This was originally demonstrated by Yoshida *et al.*, but the mechanism by which classical rotations generate these branches remains unclear.[56] Here we attempt to clarify this, beginning with a simple example: an isolated HOD molecule. In this example, there are no interactions or couplings, so the dipole correlation function $\phi(t)$ is separable into vibrational and rotational parts

$$\phi(t) = \phi_{\text{vib}}(t)\phi_{\text{rot}}(t), \tag{1}$$

with

$$\phi_{\text{vib}}(t) = \mu^2 e^{-i\omega_\upsilon t}, \tag{2}$$

$$\phi_{\text{rot}}(t) = \langle \mathbf{u}(0) \cdot \mathbf{u}(t) \rangle, \tag{3}$$

where ω_υ is the OD vibrational frequency, $\mathbf{u}$ is the transition dipole moment unit vector, which points along the OD bond, μ^2 is the oscillator strength, and $\langle \ldots \rangle$ denotes an ensemble average. If rotations are neglected, the total correlation function depends only on $\phi_{\text{vib}}(t)$, and its Fourier transform results in a single peak at ω_υ. The P and R branches must therefore originate from $\phi_{\text{rot}}(t)$.

To illustrate this, we now consider an isolated HOD molecule that is rotating freely about a fixed axis perpendicular to $\mathbf{u}$, denoted $\mathbf{u}_\perp$. This is an unphysical example, since the angular velocity is not a constant of rotational motion, but it has a pedagogical value due to its simplicity. We return to the true rotational dynamics later on. For simplicity, we neglect the ensemble average in Eq. (3) for now, using ϕ^1 to denote "correlation functions" that are not ensemble averaged: $\phi(t) = \langle \phi^1(t) \rangle$. For an isolated HOD molecule rotating about $\mathbf{u}_\perp$, $\phi^1_{\text{rot}}(t)$ is simply

$$\phi^1_{\text{rot}}(t) = \cos(\omega_r t), \tag{4}$$

where ω_r is the angular frequency of the rotation. The total dipole correlation function is then given by

$$\phi^1(t) \sim e^{-i(\omega_\upsilon + \omega_r)t} + e^{-i(\omega_\upsilon - \omega_r)t}. \tag{5}$$

Its Fourier transform gives two peaks in the spectrum at $\omega_\upsilon \pm \omega_r$. In the general case, free rotation about a fixed axis at an angle θ from $\mathbf{u}$ results in the dipole correlation function

$$\phi^1(t) \sim \cos\theta\, e^{-i\omega_\upsilon t} + \Big(1 - \cos\theta\Big)\Big(e^{-i(\omega_\upsilon + \omega_r)t} + e^{-i(\omega_\upsilon - \omega_r)t}\Big), \tag{6}$$

and its Fourier transform gives three peaks at ω_υ and $\omega_\upsilon \pm \omega_r$. After an ensemble average over all possible fixed axes of rotation and Boltzmann-weighted angular momenta, these peaks result in a spectrum with a PQR-branch structure (data not shown). The P and R branches can be understood as arising from rotations about axes that have a component perpendicular to $\mathbf{u}$ ($\theta = 90°$), while the Q branch comes from rotations about axes that have a component parallel to $\mathbf{u}$ ($\theta = 0°$).

This simple example illustrates how classical rotations can lead to the PQR-branch structure, but neglects the important fact that rotational dynamics conserve angular momentum, not angular velocity or rotational axis. A striking example of this is the so-called "tennis-racket theorem," which states that any rotation about the intermediate principal axis of an asymmetric top is unstable and will always mix with the other two rotations.[98] A simple experiment, like tossing a smartphone in the air, demonstrates this phenomenon. In the case of HOD, this means that the sinusoidal time dependence of Eq. (4) is wrong because the angular velocity is not a constant of the motion, as mentioned above. Instead, the rotational velocity trajectory evolves according to Euler's equation[99]

$$\mathbf{I}\dot{\boldsymbol{\Omega}} + \boldsymbol{\Omega} \times (\mathbf{I}\boldsymbol{\Omega}) = 0 \tag{7}$$

for an isolated rigid body, where $\boldsymbol{\Omega}$ is the vector of angular velocities and $\mathbf{I}$ is the moment of inertia tensor.

As discussed above, even though incorrect, Eq. (6) still gives a spectrum that is qualitatively correct for HOD. In the case of H_2O, on the other hand, the correct dynamics are critical. In H_2O, the two OH stretches couple, resulting in two normal modes separated by about 100 cm^{-1}, the symmetric and antisymmetric stretches. Equation (6), when applied to both normal modes of H_2O, would therefore predict a spectrum with two sharp Q branches. The vibrational lifetime of the OH stretch is 260 fs,[77] which corresponds to a width of about 20 cm^{-1}, so these two peaks should be resolved in the IR spectrum. But both the experimental[58] and calculated (Fig. 4) spectra of H_2O at low density have only one Q branch. To understand this discrepancy, we must understand the correct dynamics described by Eq. (7). These dynamics are complex and unintuitive, as demonstrated by the tennis-racket theorem, but their impact on the spectrum can be understood both by numerical solution of Eq. (7) and by decomposing the spectrum into component pieces.

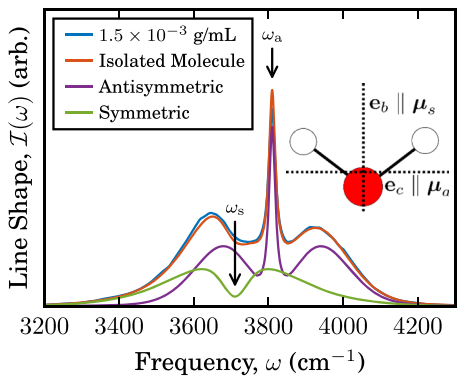

FIG. 4. The OH stretch region of the IR spectrum of neat H_2O at 673 K. The spectrum from an MD simulation at 1.5×10^{-3} g/mL (blue) is almost identical to that for an isolated molecule (orange). The total spectrum of an isolated molecule can be decomposed into contributions from the antisymmetric stretch (purple) and the symmetric stretch (green). A schematic of a water molecule (inset) shows two of the principal axes ($\mathbf{e}_b$ and $\mathbf{e}_c$) and the corresponding transition dipole moments (dotted lines). The presence and absence of a sharp peak at ω_a and ω_s, respectively, are due to the classical rotational dynamics of an asymmetric top (see text).

We begin by discussing the numerical solution of Eq. (7). One can compute the rotational correlation function $\phi_{\rm rot}(t)$ of an ensemble of isolated molecules using a simple brute force ensemble average over initial angular velocities, followed by time propagation according to Euler's equation [Eq. (7)]. The angular velocities are distributed according to the Boltzmann distribution

$$P(\mathbf{\Omega}) \sim e^{-\beta \mathbf{\Omega}^T \mathbf{I} \mathbf{\Omega}}, \tag{8}$$

with $\beta = (k_B T)^{-1}$. We sample all initial angular velocities with $P(\mathbf{\Omega}) > 10^{-8}$ on a grid with a spacing of $d\Omega = 10$ cm^{-1}. We have tested both the cutoff probability 10^{-8} and the grid spacing $d\Omega$ for convergence. We integrate Euler's equation with a fourth-order Runge-Kutta method.[100] We then calculate the spectra as described in Sec. II B.[77] This method should produce identical spectra to MD simulations in the dilute limit. We find that this agreement is achieved for simulations of neat H_2O at 1.5×10^{-3} g/mL (Fig. 4).

These numerical simulations confirm that the correct dynamics [Eq. (7)] give spectra with only a single Q branch, as observed both experimentally[58] (not shown) and in our MD simulations, but they do not explain why. This phenomenon is well understood in terms of quantum-mechanical selection rules for asymmetric-top rigid rotors,[59,60,97] but it turns out that our mixed quantum-classical approach helps to shed some light on the behavior in a more intuitive way.

In simulations of isolated molecules, there are no intermolecular couplings, so the spectrum can be cleanly decomposed into the components from the antisymmetric and symmetric stretching modes. This decomposition shows that both the antisymmetric and symmetric stretches develop rotational side bands, but the symmetric component is missing the sharp central Q band (Fig. 4). This difference can be understood in terms of the rotational correlation function. Like we did for HOD [Eq. (1)], we can likewise decompose the correlation function for an isolated, freely rotating H_2O molecule into vibrational and rotational parts

$$\phi(t) = \phi^a_{\rm vib}(t)\phi^a_{\rm rot}(t) + \phi^s_{\rm vib}(t)\phi^s_{\rm rot}(t), \tag{9}$$

where the superscripts a and s indicate the antisymmetric and symmetric modes. Without rotations, the Fourier transform of $\phi(t)$ simply gives a spectrum of two δ-function peaks at the symmetric and antisymmetric stretching frequencies, ω_a and ω_s, broadened into Lorentzians by the lifetime T_1 and with relative intensities determined by the oscillator strengths. So, to understand the shape of the spectra in Fig. 4, we must understand the behavior of the rotational correlation functions $\phi^a_{\rm rot}(t)$ and $\phi^s_{\rm rot}(t)$.

The correlation function for a vector in the molecule-fixed-frame of an arbitrary asymmetric top, rotating according to classical mechanics [Eq. (7)], is surprisingly complex and not even analytically solvable.[101] Here, we are only interested in the rotational correlation functions for the transition dipole vectors of the symmetric and antisymmetric stretching modes. In this special case, we can understand the behavior somewhat intuitively through the tennis-racket theorem.

The transition dipole of the symmetric stretch is parallel to the molecule's electric dipole, which also coincides with the $\mathbf{e}_b$ principal axis of the molecule (Fig. 4 inset). Here, the principal axes $\mathbf{e}_a$, $\mathbf{e}_b$, and $\mathbf{e}_c$ define the frame in which $\mathbf{I}$ is diagonal and correspond to the moments of inertia in decreasing order $I_a > I_b > I_c$. According to the tennis-racket theorem, rotations about the intermediate principal axes ($\mathbf{e}_b$) are unstable. So an object initially rotating about its $\mathbf{e}_b$ axis will undergo flipping motions that prohibit long-time correlations from developing for vectors that point along the $\mathbf{e}_b$ axis. Since the symmetric-stretch transition dipole moment is parallel to $\mathbf{e}_b$, $\phi^s_{\rm rot}(t)$ decays to zero, and its Fourier transform has no zero-frequency (DC) component. When convoluted with the δ-function vibrational component, this yields a line shape that has no intensity at ω_s, but has intensity on both sides.

The transition dipole of the antisymmetric stretch, on the other hand, is parallel to the $\mathbf{e}_c$ principal axis of the water molecule (Fig. 4 inset). According to the tennis-racket theorem, rotations about the $\mathbf{e}_c$ axis are stable. This means that an object initially rotating about its $\mathbf{e}_c$ axis will continue to rotate about that axis indefinitely. This allows long-time correlations to develop for vectors that point along the $\mathbf{e}_c$ axis. Since the antisymmetric stretch transition dipole is parallel to $\mathbf{e}_c$, $\phi^a_{\rm rot}(t)$ does not decay to zero, and its Fourier transform has a non-zero DC component. When convoluted with the δ-function vibrational component, this yields a spectrum that has a sharp peak at ω_a and broad bands on either side.

This behavior can be understood more quantitatively using numerical calculations of the rotational correlation functions for various vectors in the molecular frame. Such numerical correlation functions provide a general approach to understanding the effect of classical rotations on the vibrational spectra of arbitrary polyatomic molecules, from linear molecules to asymmetric tops.[102] Indeed, Guissani *et al.* found that the correlations of vectors along the $\mathbf{e}_b$ axis of an asymmetric top decay to zero, while the correlations of vectors along the $\mathbf{e}_c$ axis do not.[101]

We are now in a position to understand the spectrum of H_2O in Fig. 4. Both the symmetric and antisymmetric stretches exhibit rotational P and R bands, which sum to form the P and R bands of the H_2O spectrum. The antisymmetric stretch exhibits a Q branch centered at ω_a because rotations about the corresponding transition dipole moment are stable according to the tennis-racket theorem. The Q branch at ω_s is absent because the rotations about the corresponding transition dipole moment are unstable according to the tennis-racket theorem. In the spectrum of HOD (Fig. 2), considerations of stable and unstable rotations are not as important because the transition dipole moment along the OD bond is not parallel to the intermediate principal axes of HOD. Nevertheless, it is still important to treat the classical rotational dynamics correctly to make quantitative predictions.

While quantum-mechanical selection rules are generally rather unintuitive and abstract, the classical limit allows us to visualize the rotational dynamics responsible for the rotational structure of the IR line shape. For example, the quantum-mechanical selection rules that forbid the symmetric Q branch

from appearing in the IR spectrum can be understood classically as the instability of molecular rotations about the intermediate principal axis $\mathbf{e}_b$. In contrast, the selection rules that permit the antisymmetric Q branch correspond to the stability of molecular rotations about $\mathbf{e}_c$.

IV. CONCLUSION

We find that spectroscopic maps[72] developed for water at ambient conditions do an excellent job predicting the experimental spectra[29] of the OD stretch in supercritical water over a wide range of densities, from 1.65×10^{-2} g/mL to 1.0 g/mL. We find that the spectrum redshifts as density increases, but does not change qualitatively in the near-critical region or upon crossing the percolation line. The weak density dependence of the peak frequency at intermediate densities is a coincidence: the rotational P branch at low density happens to have a peak frequency that is similar to the high-density inhomogeneously broadened spectrum, resulting in a smooth transition between these regimes with minimal change in frequency.

We then turn to the rovibrational spectrum observed at lower densities. The mixed quantum-classical approach we use to compute the spectra not only reproduces the complex line shapes of dilute HOD in H_2O and neat H_2O but also provides some insight into the underlying chemical physics. It turns out that the forbidden Q branch in the symmetric stretch spectrum of H_2O is a quantum-mechanical manifestation of the *classical* instability of molecular rotations about the intermediate principal axis.

ACKNOWLEDGMENTS

This work was completed in part with resources provided by the University of Chicago Research Computing Center and the Institute for Molecular Engineering.

REFERENCES

[1]H. J. Bakker and J. L. Skinner, "Vibrational spectroscopy as a probe of structure and dynamics in liquid water," Chem. Rev. **110**, 1498–1517 (2010).
[2]C. Zhang, D. Donadio, and G. Galli, "First-principle analysis of the IR stretching band of liquid water," J. Phys. Chem. Lett. **1**, 1398–1402 (2010).
[3]O. Marsalek and T. E. Markland, "Quantum dynamics and spectroscopy of *ab initio* liquid water: The interplay of nuclear and electronic quantum effects," J. Phys. Chem. Lett. **8**, 1545–1551 (2017).
[4]A. P. Gaiduk, J. A. Gustafson, F. Gygi, and G. Galli, "First-principles simulations of liquid water using a dielectric-dependent hybrid functional," J. Phys. Chem. Lett. **9**, 3068 (2018).
[5]V. Rozsa, D. Pan, F. Giberti, and G. Galli, "*Ab initio* spectroscopy and ionic conductivity of water under earth mantle conditions," Proc. Natl. Acad. Sci. U. S. A. **115**, 6952 (2018).
[6]M. G. Sceats and S. A. Rice, "The intramolecular potential of water molecules engaged in hydrogen bonding from analysis of the overtone spectrum of ice I," J. Chem. Phys. **71**, 973–982 (1979).
[7]A. C. Belch and S. A. Rice, "The OH stretching spectrum of liquid water: A random network model interpretation," J. Chem. Phys. **78**, 4817–4823 (1983).
[8]L. Ojamäe, J. Tegenfeldt, J. Lindgren, and K. Hermansson, "Simulation of band widths in liquid water spectra. The breakdown of the frozen-field approximation," Chem. Phys. Lett. **195**, 97–103 (1992).
[9]U. Buck, I. Ettischer, M. Melzer, V. Buch, and J. Sadlej, "Structure and spectra of three-dimensional $(H_2O)_n$ clusters, n = 8, 9, 10," Phys. Rev. Lett. **80**, 2578–2581 (1998).
[10]V. Buch, "Molecular structure and OH-stretch spectra of liquid water surface," J. Phys. Chem. B **109**, 17771–17774 (2005).
[11]S. Corcelli, C. Lawrence, and J. L. Skinner, "Combined electronic structure/molecular dynamics approach for ultrafast infrared spectroscopy of dilute HOD in liquid H_2O and D_2O," J. Chem. Phys. **120**, 8107–8117 (2004).
[12]S. Corcelli and J. L. Skinner, "Infrared and Raman line shapes of dilute HOD in liquid H_2O and D_2O from 10 to 90 °C," J. Phys. Chem. A **109**, 6154–6165 (2005).
[13]M. Yang and J. L. Skinner, "Signatures of coherent vibrational energy transfer in IR and Raman line shapes for liquid water," Phys. Chem. Chem. Phys. **12**, 982–991 (2010).
[14]J. L. Skinner, B. M. Auer, and Y.-S. Lin, "Vibrational line shapes, spectral diffusion, and hydrogen bonding in liquid water," Adv. Chem. Phys. **142**, 59–103 (2009).
[15]B. M. Auer and J. L. Skinner, "IR and Raman spectra of liquid water: Theory and interpretation," J. Chem. Phys. **128**, 224511 (2008).
[16]C. P. Lawrence and J. L. Skinner, "Vibrational spectroscopy of HOD in liquid D_2O. II. Infrared line shapes and vibrational Stokes shift," J. Chem. Phys. **117**, 8847–8854 (2002).
[17]B. Auer, R. Kumar, J. R. Schmidt, and J. L. Skinner, "Hydrogen bonding and Raman, IR, and 2D-IR spectroscopy of dilute HOD in liquid D_2O," Proc. Natl. Acad. Sci. U.S.A. **104**, 14215 (2007).
[18]A. A. Kananenka and J. L. Skinner, "Fermi resonance in OH-stretch vibrational spectroscopy of liquid water and the water hexamer," J. Chem. Phys. **148**, 244107 (2018).
[19]C. J. Tainter, L. Shi, and J. L. Skinner, "Structure and OH-stretch spectroscopy of low- and high-density amorphous ices," J. Chem. Phys. **140**, 134503 (2014).
[20]L. Shi, S. M. Gruenbaum, and J. L. Skinner, "Interpretation of IR and Raman line shapes for H_2O and D_2O ice Ih," J. Phys. Chem. B **116**, 13821–13830 (2012).
[21]L. Shi, Y. Ni, S. E. P. Drews, and J. L. Skinner, "Dielectric constant and low-frequency infrared spectra for liquid water and ice Ih within the E3B model," J. Chem. Phys. **141**, 084508 (2014).
[22]F. Li and J. L. Skinner, "Infrared and Raman line shapes for ice Ih. I. Dilute HOD in H_2O and D_2O," J. Chem. Phys. **132**, 204505 (2010).
[23]C. J. Tainter, Y. Ni, L. Shi, and J. L. Skinner, "Hydrogen bonding and OH-stretch spectroscopy in water: Hexamer (cage), liquid surface, liquid, and ice," J. Phys. Chem. Lett. **4**, 12–17 (2013).
[24]Y. Ni and J. L. Skinner, "IR spectra of water droplets in no man's land and the location of the liquid-liquid critical point," J. Chem. Phys. **145**, 124509 (2016).
[25]M. McHugh and V. Krukonis, *Supercritical Fluid Extraction: Principles and Practice* (Butterworth–Heinemann, Stoneham, MA, 2013).
[26]A. A. Peterson, F. Vogel, R. P. Lachance, M. Fröling, M. J. J. Antal, and J. W. Tester, "Thermochemical biofuel production in hydrothermal media: A review of sub- and supercritical water technologies," Energy Environ. Sci. **1**, 32–65 (2008).
[27]H. Weingärtner and E. U. Franck, "Supercritical water as a solvent," Angew. Chem., Int. Ed. **44**, 2672–2692 (2005).
[28]P. E. Savage, "Organic chemical reactions in supercritical water," Chem. Rev. **99**, 603–622 (1999).
[29]E. U. Franck and K. Roth, "Infra-red absorption of HDO in water at high pressures and temperatures," Discuss. Faraday Soc. **43**, 108–114 (1967).
[30]G. E. Walrafen, M. S. Hokmabadi, W.-H. Yang, and G. J. Piermarini, "High-temperature high-pressure Raman spectra from liquid water," J. Phys. Chem. **92**, 4540–4542 (1988).
[31]E. U. Franck, "Water and aqueous solutions at high pressures and temperatures," Pure Appl. Chem. **24**, 13–30 (1970).
[32]J. D. Frantz, J. Dubessy, and B. Mysen, "An optical cell for Raman spectroscopic studies of supercritical fluids and its application to the study of water to 500°C and 2000 bar," Chem. Geol. **106**, 9–26 (1993).

[33]K. Downey, R. Snow, D. Hazlebeck, and A. Roberts, "Corrosion and chemical agent destruction," in *Innovations in Supercritical Fluids Science and Technology* (American Chemical Society, 1995), pp. 313–326.
[34]M. M. Hoffmann, R. S. Addleman, and J. L. Fulton, "Short-pathlength, high-pressure flow cell for static and time-resolved infrared spectroscopy suitable for supercritical fluid solutions including hydrothermal systems," Rev. Sci. Instrum. **71**, 1552–1556 (2000).
[35]P. Kritzer, "Corrosion in high-temperature and supercritical water and aqueous solutions: A review," J. Supercrit. Fluids **29**, 1–29 (2004).
[36]E. Libowitzky, "Correlation of O–H stretching frequencies and O–H. . .O hydrogen bond lengths in minerals," Monatsh. Chem. **130**, 1047–1059 (1999).
[37]R. Rey, K. B. Møller, and J. T. Hynes, "Hydrogen bond dynamics in water and ultrafast infrared spectroscopy," J. Phys. Chem. A **106**, 11993–11996 (2002).
[38]C. P. Lawrence and J. L. Skinner, "Vibrational spectroscopy of HOD in liquid D_2O. III. Spectral diffusion, and hydrogen-bonding and rotational dynamics," J. Chem. Phys. **118**, 264–272 (2003).
[39]C. J. Fecko, J. D. Eaves, J. J. Loparo, A. Tokmakoff, and P. L. Geissler, "Ultrafast hydrogen-bond dynamics in the infrared spectroscopy of water," Science **301**, 1698–1702 (2003).
[40]G. O. Jones and P. A. Walker, "Specific heats of fluid argon near the critical point," Proc. Phys. Soc., London, Sect. B **69**, 1348 (1956).
[41]L. Xu, P. Kumar, S. V. Buldyrev, S.-H. Chen, P. H. Poole, F. Sciortino, and H. E. Stanley, "Relation between the Widom line and the dynamic crossover in systems with a liquid-liquid phase transition," Proc. Natl. Acad. Sci. U. S. A. **102**, 16558–16562 (2005).
[42]F. Sciortino, P. H. Poole, U. Essmann, and H. E. Stanley, "Line of compressibility maxima in the phase diagram of supercooled water," Phys. Rev. E **55**, 727–737 (1997).
[43]J. L. F. Abascal and C. Vega, "Widom line and the liquid-liquid critical point for the TIP4P/2005 water model," J. Chem. Phys. **133**, 234502 (2010).
[44]F. Gorelli, M. Santoro, T. Scopigno, M. Krisch, and G. Ruocco, "Liquidlike behavior of supercritical fluids," Phys. Rev. Lett. **97**, 245702 (2006).
[45]T. Morita, K. Kusano, H. Ochiai, K.-i. Saitow, and K. Nishikawa, "Study of inhomogeneity of supercritical water by small-angle x-ray scattering," J. Chem. Phys. **112**, 4203–4211 (2000).
[46]G. G. Simeoni, T. Bryk, F. A. Gorelli, M. Krisch, G. Ruocco, M. Santoro, and T. Scopigno, "The Widom line as the crossover between liquid-like and gas-like behaviour in supercritical fluids," Nat. Phys. **6**, 503–507 (2010).
[47]M. Y. Ha, T. J. Yoon, T. Tlusty, Y. Jho, and W. B. Lee, "Widom delta of supercritical gas-liquid coexistence," J. Phys. Chem. Lett. **9**, 1734–1738 (2018).
[48]P. Schienbein and D. Marx, "Investigation concerning the uniqueness of separatrix lines separating liquid-like from gas-like regimes deep in the supercritical phase of water with a focus on Widom line concept," Phys. Rev. E **98**, 022104 (2018).
[49]Y. D. Fomin, V. Ryzhov, E. Tsiok, and V. Brazhkin, "Thermodynamic properties of supercritical carbon dioxide: Widom and Frenkel lines," Phys. Rev. E **91**, 022111 (2015).
[50]S. E. Strong, L. Shi, and J. L. Skinner, "Percolation in supercritical water: Do the Widom and percolation lines coincide?," J. Chem. Phys. **149**, 084504 (2018).
[51]T. J. Yoon, M. Y. Ha, W. B. Lee, and Y.-W. Lee, "Probabilistic characterization of the Widom delta in supercritical region," J. Chem. Phys. **149**, 014502 (2018).
[52]S. Mukamel, P. S. Stern, and D. Ronis, "Universality in the critical broadening of spectral lines in simple fluids," Phys. Rev. Lett. **50**, 590–594 (1983).
[53]M. Musso, F. Matthai, D. Keutel, and K.-L. Oehme, "Isotropic Raman line shapes near gas-liquid critical points: The shift, width, and asymmetry of coupled and uncoupled states of fluid nitrogen," J. Chem. Phys. **116**, 8015–8027 (2002).
[54]S. A. Egorov, C. P. Lawrence, and J. L. Skinner, "A mode-coupling theory of vibrational line broadening in near-critical fluids," J. Phys. Chem. B **109**, 6879–6883 (2005).
[55]R. Kubo, "A stochastic theory of line shape," Adv. Chem. Phys. **15**, 101–127 (1969).
[56]K. Yoshida, N. Matubayasi, Y. Uosaki, and M. Nakahara, "Density effect on infrared spectrum for supercritical water in the low- and medium-density region studied by molecular dynamics simulation," J. Chem. Phys. **137**, 194506 (2012).
[57]K. Yoshida, N. Matubayasi, Y. Uosaki, and M. Nakahara, "Effect of heavy hydrogen isotopes on the vibrational line shape for supercritical water through rotational couplings," J. Chem. Phys. **138**, 134508 (2013).
[58]G. V. Bondarenko and Y. E. Gorbaty, "An infrared study of water vapour in the temperature range 573-723 K. Dimerization enthalpy and absorption intensities for monomer and dimer," Mol. Phys. **74**, 639–647 (1991).
[59]D. M. Dennison, "The infrared spectra of polyatomic molecules. I," Rev. Mod. Phys. **3**, 280–345 (1931).
[60]G. Herzberg, *Molecular Spectra and Molecular Structure: II. Infrared and Raman Spectra of Polyatomic Molecules* (D. Van Nostrand Company, New York, 1945).
[61]J. L. F. Abascal and C. Vega, "A general purpose model for the condensed phases of water: TIP4P/2005," J. Chem. Phys. **123**, 234505 (2005).
[62]C. Vega, J. L. F. Abascal, and I. Nezbeda, "Vapor-liquid equilibria from the triple point up to the critical point for the new generation of TIP4P-like models: TIP4P/Ew, TIP4P/2005, and TIP4P/ice," J. Chem. Phys. **125**, 034503 (2006).
[63]C. J. Tainter, L. Shi, and J. L. Skinner, "Reparametrized E3B (explicit three-body) water model using the TIP4P/2005 model as a reference," J. Chem. Theory Comput. **11**, 2268–2277 (2015).
[64]S. Miyamoto and P. A. Kollman, "SETTLE: An analytical version of the SHAKE and RATTLE algorithm for rigid water models," J. Comput. Chem. **13**, 952–962 (1992).
[65]R. W. Hockney, S. P. Goel, and J. W. Eastwood, "Quiet high-resolution computer models of a plasma," J. Comput. Phys. **14**, 148–158 (1974).
[66]S. Nosé, "A unified formulation of the constant temperature molecular dynamics methods," J. Chem. Phys. **81**, 511–519 (1984).
[67]W. G. Hoover, "Canonical dynamics: Equilibrium phase-space distributions," Phys. Rev. A **31**, 1695–1697 (1985).
[68]U. Essmann, L. Perera, M. L. Berkowitz, T. Darden, H. Lee, and L. G. Pedersen, "A smooth particle mesh Ewald method," J. Chem. Phys. **103**, 8577–8593 (1995).
[69]S. Pronk, S. Páll, R. Schulz, P. Larsson, P. Bjelkmar, R. Apostolov, M. R. Shirts, J. C. Smith, P. M. Kasson, D. van der Spoel, B. Hess, and E. Lindahl, "GROMACS 4.5: A high-throughput and highly parallel open source molecular simulation toolkit," Bioinformatics **29**, 845–854 (2013).
[70]S. E. Strong and J. D. Eaves, "Atomistic hydrodynamics and the dynamical hydrophobic effect in porous graphene," J. Phys. Chem. Lett. **7**, 1907–1912 (2016).
[71]S. Plimpton, "Fast parallel algorithms for short-range molecular dynamics," J. Comput. Phys. **117**, 1–19 (1995).
[72]S. M. Gruenbaum, C. J. Tainter, L. Shi, Y. Ni, and J. L. Skinner, "Robustness of frequency, transition dipole, and coupling maps for water vibrational spectroscopy," J. Chem. Theory Comput. **9**, 3109–3117 (2013).
[73]T. Steinel, J. B. Asbury, J. Zheng, and M. Fayer, "Watching hydrogen bonds break: A transient absorption study of water," J. Phys. Chem. A **108**, 10957–10964 (2004).
[74]S. Corcelli, C. Lawrence, J. Asbury, T. Steinel, M. Fayer, and J. L. Skinner, "Spectral diffusion in a fluctuating charge model of water," J. Chem. Phys. **121**, 8897–8900 (2004).
[75]Y. Ni and J. L. Skinner, "Ultrafast pump-probe and 2DIR anisotropy and temperature-dependent dynamics of liquid water within the E3B model," J. Chem. Phys. **141**, 024509 (2014).
[76]J. R. Schmidt, S. T. Roberts, J. J. Loparo, A. Tokmakoff, M. D. Fayer, and J. L. Skinner, "Are water simulation models consistent with steady-state and ultrafast vibrational spectroscopy experiments?," Chem. Phys. **341**, 143–157 (2007).
[77]A. J. Lock and H. J. Bakker, "Temperature dependence of vibrational relaxation in liquid H_2O," J. Chem. Phys. **117**, 1708–1713 (2002).

[78]W. S. Benedict, N. Gailar, and E. K. Plyler, "Rotation-vibration spectra of deuterated water vapor," J. Chem. Phys. **24**, 1139–1165 (1956).
[79]J. B. Asbury, T. Steinel, C. Stromberg, S. Corcelli, C. Lawrence, J. L. Skinner, and M. Fayer, "Water dynamics: Vibrational echo correlation spectroscopy and comparison to molecular dynamics simulations," J. Phys. Chem. A **108**, 1107–1119 (2004).
[80]J. Schmidt, S. Corcelli, and J. L. Skinner, "Pronounced non-Condon effects in the ultrafast infrared spectroscopy of water," J. Chem. Phys. **123**, 044513 (2005).
[81]J. J. Loparo, S. T. Roberts, R. A. Nicodemus, and A. Tokmakoff, "Variation of the transition dipole moment across the OH stretching band of water," Chem. Phys. **341**, 218–229 (2007).
[82]H. Ma and J. Ma, "Density dependence of hydrogen bonding and the translational-orientational structural order in supercritical water: A molecular dynamics study," J. Chem. Phys. **135**, 054504 (2011).
[83]I. Skarmoutsos, E. Guardia, and J. Samios, "Local structural fluctuations, hydrogen bonding and structural transitions in supercritical water," J. Supercrit. Fluids **130**, 156–164 (2017).
[84]We compute the unpolarized Raman spectra with the polarizability maps in Ref. 72.
[85]Y. Ikushima, K. Hatakeda, N. Saito, and M. Arai, "An *in situ* Raman spectroscopy study of subcritical and supercritical water: The peculiarity of hydrogen bonding near the critical point," J. Chem. Phys. **108**, 5855–5860 (1998).
[86]K. Yui, H. Uchida, K. Itatani, and S. Koda, "Raman OH stretching frequency shifts in supercritical water and in O_2- and acetone-aqueous solutions near the water critical point," Chem. Phys. Lett. **477**, 85–89 (2009).
[87]Y. Yasaka, M. Kubo, N. Matubayasi, and M. Nakahara, "High-sensitivity Raman spectroscopy of supercritical water and methanol over a wide range of density," Bull. Chem. Soc. Jpn. **80**, 1764–1769 (2007).
[88]S. S. Xantheas, "Cooperativity and hydrogen bonding network in water clusters," Chem. Phys. **258**, 225–231 (2000).
[89]C. J. Tainter, P. A. Pieniazek, Y.-S. Lin, and J. L. Skinner, "Robust three-body water simulation model," J. Chem. Phys. **134**, 184501 (2011).
[90]F. Weinhold, "Quantum cluster equilibrium theory of liquids: Illustrative application to water," J. Chem. Phys. **109**, 373–384 (1998).
[91]P. Wernet, D. Nordlund, U. Bergmann, M. Cavalleri, M. Odelius, H. Ogasawara, L. Å. Näslund, T. K. Hirsch, L. Ojamäe, P. Glatzel, L. G. M. Pettersson, and A. Nilsson, "The structure of the first coordination shell in liquid water," Science **304**, 995–999 (2004).
[92]N. J. Hestand and J. L. Skinner, "Perspective: Crossing the Widom line in no man's land: Experiments, simulations, and the location of the liquid-liquid critical point in supercooled water," J. Chem. Phys. **149**, 140901 (2018).
[93]A. Manka, H. Pathak, S. Tanimura, J. Wölk, R. Strey, and B. E. Wyslouzil, "Freezing water in no-man's land," Phys. Chem. Chem. Phys. **14**, 4505–4516 (2012).
[94]A. J. Amaya and B. E. Wyslouzil, "Ice nucleation rates near 225 K," J. Chem. Phys. **148**, 084501 (2018).
[95]D. Corradini, M. Rovere, and P. Gallo, "The Widom line and dynamical crossover in supercritical water: Popular water models versus experiments," J. Chem. Phys. **143**, 114502 (2015).
[96]E. W. Lemmon, "Thermophysical properties of fluids," in *NIST Chemistry WebBook* (CRC Press, 2009), www.nist.gov/publications/thermophysical-properties-fluids; accessed May 5, 2018.
[97]H. N. Ritland, "The infrared absorption spectrum of water vapor and carbon dioxide," Technical Report No. LMSC-3-77-62-2, Lockheed Missles and Space Division, 1962.
[98]M. S. Ashbaugh, C. C. Chicone, and R. H. Cushman, "The twisting tennis racket," J. Dyn. Differ. Equation **3**, 67–85 (1991).
[99]H. Goldstein, C. P. Poole, Jr., and J. L. Safko, *Classical Mechanics*, 3rd ed. (Pearson, San Francisco, 2001).
[100]W. H. Press, S. A. Teukolsky, W. T. Vetterling, and B. P. Flannery, *Numerical Recipes: The Art of Scientific Computing*, 3rd ed. (Cambridge University Press, New York, 2007).
[101]Y. Guissani, J. C. Leicknam, and S. Bratos, "Vectorial correlation functions for a classical system of free asymmetric rotors," Phys. Rev. A **16**, 2072–2079 (1977).
[102]J. C. Leicknam, Y. Guissani, and S. Bratos, "Infrared study of diluted solutions of polyatomic molecules. I. Band shape of fundamentals associated with nondegenerate normal modes," J. Chem. Phys. **68**, 3380–3390 (1978).